

Three regimes of a picosecond magnetoacoustics in ferromagnetic structures

P. I. Gerevenkov,^{1,*} Ia. A. Mogunov,¹ Ia. A. Filatov,¹ N. S. Gusev,²
M. V. Sapozhnikov,² N. E. Khokhlov,¹ and A. M. Kalashnikova¹

¹*Ioffe Institute, 194021 St. Petersburg, Russia*

²*IPM RAS, 603950 Nizhny Novgorod, Russia*

(Dated: May 30, 2025)

The development of magnonic devices requires energy-efficient methods for generating spin waves and controlling their parameters. Acoustic waves are known to excite spin waves resonantly with magneto-elastic wave formation or to drive non-resonantly forced magnetization oscillations. Short acoustic wavepackets enable another resonant interaction regime - Cherenkov radiation of spin waves. This poses a question on the criteria and signatures of transitions between these three regimes of a picosecond magnetoacoustic. Here, we use the scanning magneto-optical pump-probe technique to directly reveal all three regimes of interactions of laser-driven acoustic and magnetostatic wave packets in a thin permalloy film and a waveguide on top of a (011)-Si substrate. Direct measurements of the phase velocities revealed the transition from coupled magneto-elastic wavepacket to Cherenkov-like radiation and non-resonant regime controlled by the detuning between magnon and phonon group velocities. Acoustic pulse is found to be affected by the excited magnetization dynamics only in the magneto-elastic regime.

Increasing demands for computing efficiency stimulate the quest for new ways of processing information. Over the past few years, prototypes and concepts for the construction of full-fledged computing devices have emerged in magnonics [1, 2]. In particular, it has been demonstrated [3] that the available magnonic elements, such as half-adder [4], diode [5] and a majority element [6], constitute a sufficient set for conventional digital computing. Several unconventional computing methods employing magnonics are actively being developed, such as neuromorphic and reservoir computing [7–9]. All these approaches are heavily dependent on the magnetostatic spin waves (MSW). Recent micromagnetic simulations predict the superiority of magnonic computation over classical 7-nm CMOS technologies [10] but require improved MSW excitation efficiency, pulsed operation mode, and easy integration with existing CMOS and electronic components.

One of the promising directions to meet these requirements is to utilize the coupling between MSW and a surface acoustic wave (SAW) which allows acoustic control of spin wave parameters with superior energy efficiency (see ch. 8 of [11], ch. 10 of [12] and [13–16]) and selectivity to various acoustic modes [17–19]. The MSW-SAW coupling is also a source of nonlinearity that does not require large dynamic amplitudes and can be used for reservoir computing [20]. The propagation of an acoustic pulse in a magnetic layer can lead to two distinct resonant effects: i) the formation of a coupled magneto-elastic (ME) wave (also called a magnon-polaron) demonstrated both in bulk [21, 22] and on a surface [19, 23–25]; and ii) the excitation of a MSW by the Cherenkov-like process without a significant modification of the exciting acoustic pulse demonstrated only recently in a bulk magnet [26]. In

both effects, the energy transfer between a spin wave and lattice oscillations is realized through the same magnetoelastic coupling constants. The aforementioned raises a fundamental question: are the magneto-elastic wave formation and spin wave emission via a Cherenkov-like process the same phenomenon?

In this Letter, using laser-induced acoustic wavepackets, we experimentally demonstrate transition between Cherenkov-type spin wave emission and magnetoelastic wavepacket formation when the spin wave dispersion of the ferromagnetic layer changes from backward volume to surface waves. Using a theoretical model, the transition between these resonant regimes is associated with a detuning between the acoustic and spin wave group velocities. In addition, a non-resonant regime of forced magnetization oscillations was identified. A T-shaped waveguide with a magnetization direction gradient is used to demonstrate the transition between regimes during the acoustic wavepacket propagation.

We used as a sample polycrystalline permalloy $\text{Ni}_{80}\text{Fe}_{20}$ (Py) film with thickness $d = 20$ nm deposited on a monocrystalline (011)-Si substrate. A T-shaped waveguide with width of $5\text{ }\mu\text{m}$, etched from the same permalloy film, is used as a structure with a non-uniform distribution of the magnetization direction (Sec. I in Suppl. Material [27]). Experiments were performed using an all-optical space- and time-resolved pump-probe technique with probe reflectivity and polarization plane rotation measurements (Sec. II in Suppl. Material [27]). Excitation was performed at the edge of the Py film (Fig. 1 a), allowing excitation and detection of wavenumbers k up to $2\text{ }\mu\text{m}^{-1}$ [28, 29]. Magnetic field H_{ext} was applied in the structures plane. We used the micromagnetic simulation to determine the MSW dispersion under conditions of an inhomogeneous magnetization direction distribution [30] (Sec. III in Suppl. Material [27]).

To determine the generated SAW modes we performed probe polarization plane rotation detection of laser-

* petr.gerevenkov@mail.ioffe.ru; <http://www.ioffe.ru/ferrolab/>

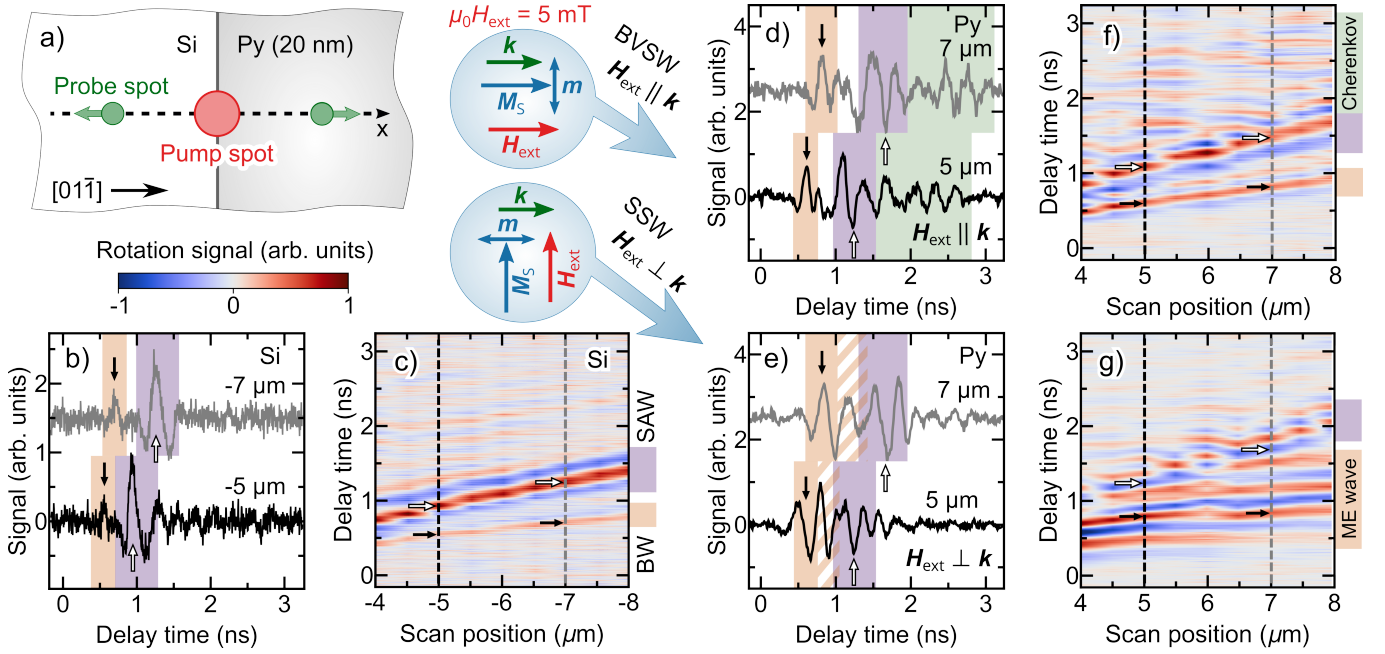


FIG. 1. **Acoustic and magnetostatic waves in Py film on Si substrate.** (a) Excitation and detection sketch. (b) Pump-probe signals in Si at different distances from the excitation spot. Color area highlights wavepackets propagating with different group velocity. Arrows mark equal points in each wavepacket. (c) Map of pump-probe signal in Si vs distance and delay time between excitation and detection. (d,e) Pump-probe signals in Py film at different distances from the excitation spot for external magnetic field along (d) and across (e) the propagation direction. Green area in panel (d) highlight additional dynamics. (f,g) Maps of pump-probe signal in Py for external magnetic field along (f) and across (g) the propagation direction.

induced waves in a bare (011)-Si substrate. SAWs were generated through the thermoelastic mechanism upon excitation of the edge of the Py film (Fig. 1 a). The signals measured at two distances from the excitation area are shown in Fig. 1 b. Two short wavepackets propagate with different group velocities (highlighted by colored areas). The wavepackets are observed in both rotation and reflectivity data (Sec. IV Suppl. Materials [27]) and their shapes do not change during propagation, indicating the absence of group velocity dispersion [31]. This allows us to directly measure the phase velocity by tracking a certain point in the waveform (the arrows in Fig. 1 b,c). For bare Si substrate in a high-symmetry propagation direction such as $[01\bar{1}]$ one expects quasi-Rayleigh mode (R-SAW) with elliptically-polarized atomic motion in a plane parallel to the acoustic wave vector k_{SAW} and surface normal [32, 33] (Sec. IV in Suppl. Materials [27]). It is also common to detect a bulk longitudinal acoustic wave (BW) propagating under the surface and comprising an atomic motion similar to R-SAW [34, 35]. Thus, we classify a packet that propagates at a lower speed (6.0 km/s) as a R-SAW, and one that propagates at a higher speed (10.3 km/s) as a BW. Note that the maximum spectral amplitude of the BW/SAW is at 3.6 GHz.

Now, we consider the propagation of waves from the same excitation spot into a Si capped with ferromagnetic film (Fig. 1 a). The presence of Py film enables additional Love acoustic mode (L-SAW) with linearly-polarized in-plane atomic motion perpendicular to k_{SAW} [32] (Sec. IV,

V in Suppl. Materials [27]). The ferromagnetic Py layer also enables surface (SSW) and backwards volume (BVSW) magnetostatic waves [3], which polarization m depends on the equilibrium magnetization direction M_S [18]. In the experiment, we again observe two acoustic wavepackets (Fig. 1 d,e) the velocities of which are slightly different from the case of bare Si substrate due to mechanical loading by a Py layer [27, 36]. In the BVSW geometry ($H_{\text{ext}} \parallel k$), there are additional oscillations following the SAW wavepacket (marked by a green area in Fig. 1 d,f). The emerging of a spin wave following an acoustic pulse corresponds to the Cherenkov-like emission of MSW reported recently for bulk acoustic and spin waves [26]. In the SSW geometry ($H_{\text{ext}} \perp k$) such an excitation is not observed, instead there is a significant broadening of the BW packet (indicated by the striped area in Fig. 1 e). The broadening is a result of the BW phase velocity increase to $20.3 \div 39$ km/s for different parts of the wavepacket. This behavior is characteristic for nonlinear dispersion, which is indicative of the propagating ME wave formation. Additionally, the signal-to-noise ratio is significantly higher for all wavepackets as compared to the bare substrate case that may stem from detection mediated by forced magnetization dynamics.

To support the suggested scenarios, we employ theoretical analysis. The acoustic wavepacket is approximated by an effective field perturbation via magnetoelastic coupling (Sec. VI of Suppl. Material [27]). BW/SAW packets cause a localized LL-torque $T(x)$ acting on magnetiza-

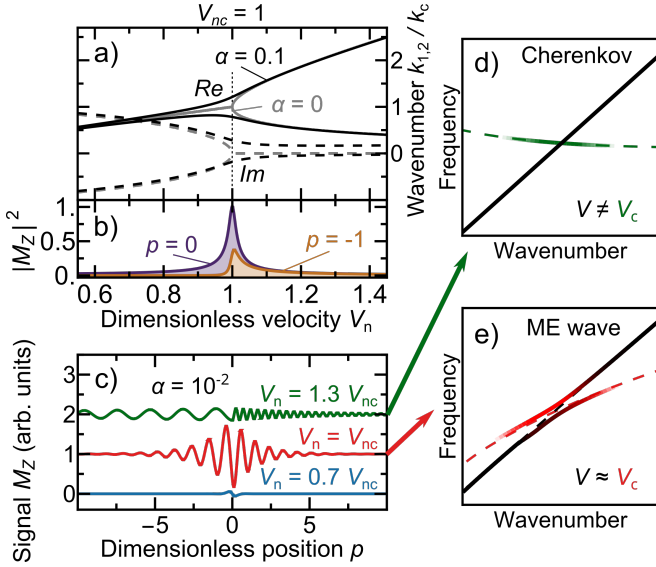


FIG. 2. **Different interaction regimes between acoustic and magnetic wavepackets.** (a) Dependences of real (solid lines) and imaginary (dashed lines) parts of the two roots $k_{1,2}$ of Eq. (1) on the dimensionless sound velocity for low (gray) and high (black) Gilbert damping. (b) Squared magnetization dynamics magnitude vs. dimensionless velocity for two positions from the center of the acoustic wavepacket $p = \tilde{x}k_c$. (c) Magnetic dynamics excited by a acoustic pulse moving with velocity above (green), equal (red) or below (blue) the critical value. (d) Illustration of the Cherenkov-like excitation regime, when acoustic and spin wave group velocities differ significantly, and (e) the magneto-elastic wave formation at a near-tangent intersection.

tion. The torque magnitude depends on the relative polarizations of the acoustic and magnetostatic waves [18], while their overlap across the film thickness is assumed to be maximal, as $kd \ll 1$ [37]. The torque moves at the acoustic velocity v through a medium characterized by a spin-wave dispersion $f(k)$. We use the Taylor expansion for $f(k)$ near the point k_c of the tangent intersection of acoustic and spin wave dispersion. The corresponding critical velocity $f'(k_c) = f(k_c)/k_c = v_c$. Then we obtain the solution for the dynamic magnetization m :

$$\begin{aligned}
 m(\tilde{x}) &= T(\tilde{x}) * \frac{1}{k_1 - k_2} \{ e^{2\pi i k_1 \tilde{x}} \Theta[\tilde{x} S_{\Im}(k_1)] S_{\Im}(k_1) - \\
 &\quad - e^{2\pi i k_2 \tilde{x}} \Theta[\tilde{x} S_{\Im}(k_2)] S_{\Im}(k_2) \}, \\
 k_{1,2} &= k_c \left(\Xi(v_n) \pm \sqrt{\Xi(v_n)^2 - 1} \right), \\
 \Xi(v_n) &= v_n \frac{1 + i\alpha}{1 + \alpha^2} - v_{nc} + 1,
 \end{aligned} \tag{1}$$

where $\tilde{x} = x - vt$ is a distance from the center of the LL-torque profile in the moving coordinate system, asterisk denotes a convolution operation, $k_{1,2}$ are the wavenumbers of two spin-waves, $\Theta(x)$ is a Heaviside function, $S_{\Im}(x)$ is a sign of $\text{Im}(x)$, $v_n = v/[k_c f''(k_c)]$ and $v_{nc} = v_c/[k_c f''(k_c)]$ are dimensionless acoustic velocities.

Expressions (1) describe three regimes of the interaction, as illustrated in Fig. 2a, where the dimensionless critical velocity is taken to be $v_{nc} = 1$. In Fig. 2c we plot spatial dynamics of m in the three regimes:

- BW/SAW and MSW dispersion curves intersect, and $v_n > v_{nc}$ ($v \neq v_c$). In this case, their group velocities strongly differ, and spin waves with k_1 and k_2 are emitted from the acoustic wavepacket area (green line in Fig. 2c), decaying in space with only intrinsic damping (dashed lines in Fig. 2a). These waves propagate ahead/behind the excitation pulse in accordance with their group velocities [38, 39]. As a result, within the pulse area, the magnetization dynamics amplitude is small (Fig. 2b) and no reciprocal effect on the acoustic pulse is expected. This is a **Cherenkov-like** regime.
- BW/SAW and MSW dispersion curves are tangent, $v_n \approx v_{nc}$. The excited spin wave becomes degenerate with a single wavenumber $k = k_c$ (at $\alpha = 0$). There is an additional spatial localization of magnetization dynamics around the excitation pulse (red line in Fig. 2c) and an increase of its maximum amplitude (Fig. 2b). In this case, a propagating **magneto-elastic wave** can be formed. We note that the enhancement of the spin wave amplitude upon change of the localized source velocity to $v \approx v_c$ was reported in [40].
- BW/SAW and MSW dispersions have no shared points and $v_n < v_{nc}$. Hence, only **non-resonant** interaction is possible. In this case forced magnetization dynamics is seen only within the acoustic wavepacket (see blue curve in Fig. 2c). We attribute the increase in signal-to-noise ratio in the Py-capped substrate (Fig. 1d,e) to the detection of acoustic wavepackets through the magnetic system. This interaction allows one to selectively detect acoustic wave packets by choosing the magnetization direction, as we demonstrate below.

Increasing α results in a smoothing of the transition between the scenarios (see the gray and black curves in Fig. 2a). The conditions for the three regimes can be generalized beyond the vicinity of k_c to be applied to the experimental observations. In Fig. 2d, Cherenkov regime is enabled in the vicinity of the intersection of BVSW and SAW dispersions, where their group velocities differ strongly. In the vicinity of the intersection of the SSW and SAW dispersions, the condition for ME wave formation is fulfilled, as the group velocities are close (Fig. 2e). Farther from the intersections, a non-resonant regime is realized. Note that Fig. 2c shows dependences of m obtained from Eq. (1) under assumption $T(\tilde{x}) = \delta(\tilde{x})$. For a realistic torque shape with a micron length, a suppression of the high-wavenumber part is expected [26]. Indeed, in the experiment, the Cherenkov-like excited BVSW is clearly observed only after the SAW pulse (Fig. 1f).

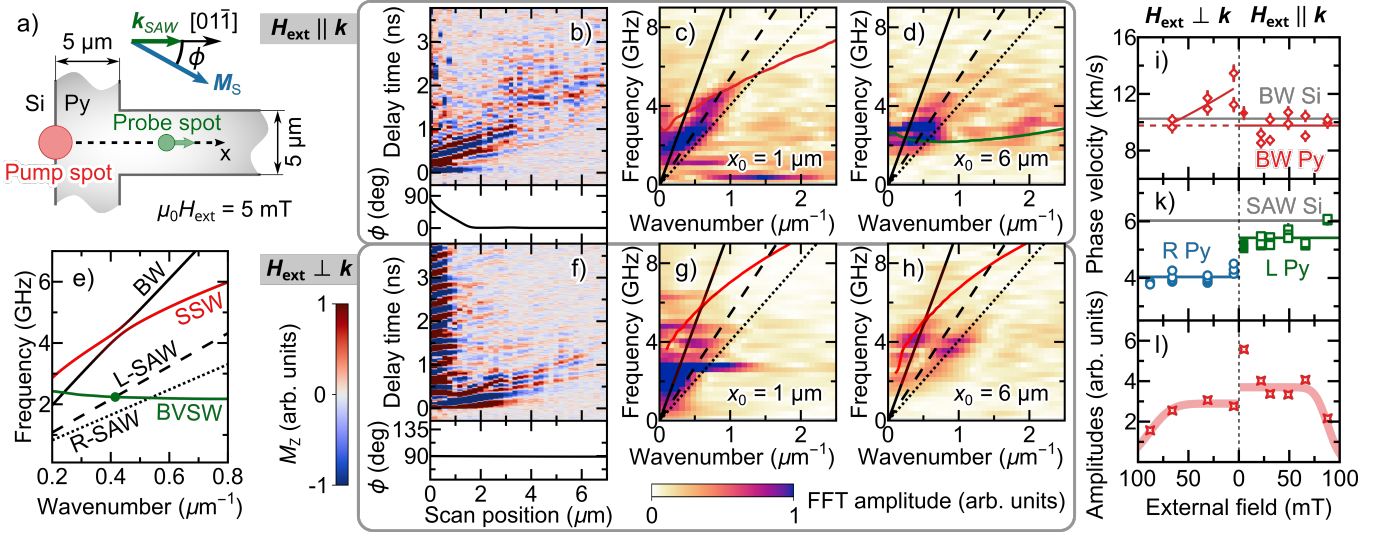


FIG. 3. **Acoustic and magnetic waves in a T-shaped magnonic waveguide with magnetization direction gradient.** (a) Excitation and detection sketch. (b,f) Signal maps vs distance and delay time between excitation and detection for external magnetic field along (b) and across (f) the propagation direction. The bottom panels show the corresponding angles of the magnetization direction relative to the \mathbf{k}_{SAW} , obtained using micromagnetic simulation. (c,d) and (g,h) show a window 2D FFT of data from Fig. 3b and f, respectively. The Gaussian-shape space window with FWHM = $2.4 \mu\text{m}$ placed at 1 (c,g) or $6 \mu\text{m}$ (d,h) from the pump area. (e) Dispersion relations of reconstructed using phase velocity values acoustic wavepackets (black), SSW (red) and BVSW (green) obtained from micromagnetic simulation. (i,k) Phase velocities of BW (i), R- and L-SAW (k) wavepackets, measured with external magnetic field across (SSW geometry) and along (BVSW geometry) the propagation direction. Corresponding values in pure (011)-Si substrate shown by gray lines. (l) Dependence of integrated window 2D FFT data at $6 \mu\text{m}$ amplitudes vs. magnetic field.

To demonstrate the transition between interaction regimes in a course of the acoustic pulse propagation, we use the T-shaped waveguide with nonuniform equilibrium magnetization direction (Fig. 3a). The dependences of the \mathbf{M}_S direction relative to the waveguide axis ϕ in an external magnetic field $\mu_0 H_{\text{ext}} = 5 \text{ mT}$ were calculated using micromagnetic simulation. As seen in a bottom panels of Fig. 3b,f, at $\mathbf{H}_{\text{ext}} \parallel \mathbf{k}$, a gradual transition from the SSW ($\phi = 90^\circ$) to the BVSW ($\phi = 0^\circ$) geometry is expected [41–43], while at $\mathbf{H}_{\text{ext}} \perp \mathbf{k}$ only the SSW regime is realized. In the range of $x=4\text{--}7 \mu\text{m}$, the \mathbf{M}_S no longer depends on x for both geometries, so this range was used to measure wavepackets phase velocity (Sec. VII in Suppl. Material [27]).

The spatio-temporal map of the magneto-optical response in the $\mathbf{H}_{\text{ext}} \parallel \mathbf{k}$ geometry is shown in Fig. 3b. The propagation of the SAW wavepacket is detected at distances up to $x = 3 \mu\text{m}$. At larger distances, the SAW is no longer detectable, while MSW emerges, excited by the SAW wavepacket via a Cherenkov-like process, similar to Fig. 1f. This indicates the change of interaction regime at $x = 3 \mu\text{m}$ from non-resonant to Cherenkov-like, concomitant with the 90° rotation of \mathbf{M}_S . Fig. 3c,d show the color-coded dispersion obtained using window-FFT from Fig. 3b, near the excitation area (at a distance of $x_0 = 1 \mu\text{m}$, panel c) and far from it ($x_0 = 6 \mu\text{m}$, panel d). They are plotted along with the dispersions of the non-interacting spin and acoustics waves. Around the excitation area we see the SAW packet propagation with

close to linear dispersion (dark area in Fig. 3c). Far from the point of excitation (Fig. 3d) we see a localization of the excited MSW amplitudes around the SAW–MSW dispersions intersection point where $v \neq v_c$. This confirms that the Cherenkov-like MSW emission seen in Fig. 3b originates from the SAW wavepacket. Cherenkov-like regime is observed only in low applied field values. An increase in H_{ext} shifts the intersection point to higher frequencies where the acoustic spectral amplitude decreases. Fig. 3k shows the values of the SAW phase velocities vs. \mathbf{H}_{ext} value. The filled point at $H_{\text{ext}} = 5 \text{ mT}$ in the BVSW geometry correspond to SAW phase velocities extracted from optical reflectivity measurements (Sec. VIII in Suppl. Material [27]). As can be seen, the Cherenkov-like regime does not affect the SAW phase velocity. The emission of an additional BVSW by the SAW wavepacket leads to an increase in the integrated dynamic amplitudes at $H_{\text{ext}} = 5 \text{ mT}$ (shown for $x_0 = 6 \mu\text{m}$ in Fig. 3l).

In the $\mathbf{H}_{\text{ext}} \perp \mathbf{k}$ geometry (Fig. 3f) we observe the SAW wavepacket in the whole range of distances. Near the excitation area (Fig. 3g), the contribution of ferromagnetic resonance dominates, which is typical when magnetization is aligned with easy anisotropy direction [31]. At a $6 \mu\text{m}$ distance we see two wavepackets (Fig. 3h). In the detectable k range, only the SSW and BW dispersions intersect with $v \approx v_c$ (Fig. 3e). One of the wavepackets clearly corresponds to the this intersection. The formation of coherent ME wavepacket usually manifests itself in by the occurrence dispersions anticrossing [37, 44, 45].

In the case of short wavepackets, their spectral width (about 1 GHz) exceeds the highest reported splitting values [25, 37, 44, 45]. Therefore, to prove the ME nature of the wavepacket, we use the fact that the interaction modifies the SSW and BW dispersion curves, leading to dependency of the BW phase velocity on the H_{ext} (Sec. IX of Suppl. Material [27]). Indeed BW phase velocity increases with decreasing H_{ext} .

At higher fields only non-resonant regime of interaction is realized for the BW/SAW wavepacket. In Fig. 3k it can be seen that the phase velocity of the SAW is different in the $\mathbf{H}_{\text{ext}} \parallel \mathbf{k}$ and $\mathbf{H}_{\text{ext}} \perp \mathbf{k}$ geometries. This is due to the fact that the polarization \mathbf{m} directed orthogonally to \mathbf{k}_{SAW} effectively interacts with L-SAW, whereas $\mathbf{m} \parallel \mathbf{k}_{\text{SAW}}$ couples to R-SAW. Increasing the field results in further increase in the frequency difference between the acoustic and magnetostatic dispersions, leading to suppression of the integrated dynamic amplitudes (Fig. 3l). Thus, L/R-SAW in our experiment are detected selectively depending on the direction of \mathbf{H}_{ext} due to a non-resonant interaction with the magnetization in Py layer.

In summary, we experimentally realized three regimes of the propagation and interaction between picosecond acoustic wavepackets traveling predominantly in the substrate and magnetization in a thin ferromagnetic film on its surface. Cherenkov-like radiation of a narrow-spectrum MSW takes place without significant impact on the exciting acoustic wavepacket. The formation of

a propagating magneto-elastic wave manifests itself in high-amplitude magnetic dynamics localized around the acoustic pulse and modifying acoustic pulse as well. The non-resonant regime shows low-amplitude forced magnetic oscillations enabling selective detection of different acoustic modes with improved sensitivity. The realization of a specific resonant regime is determined by the detuning between the MSW and BW/SAW group velocities at the intersection point of their dispersions or by proximity of the dispersions in the case of a non-resonant regime. Our experimental results in a waveguide with a non-uniform equilibrium magnetization direction demonstrate switching between interaction regimes even in a course of the acoustic pulse propagation, as well as changing the predominant magnetoacoustic coupling from one SAW mode to another by changing the equilibrium magnetization direction.

ACKNOWLEDGMENTS

The work of P.I.G. was supported by the grant of the RSF No. 24-72-00136, <https://rscf.ru/project/24-72-00136/>. The sample technology development and fabrication were done by N.S.G. and M.V.S. in the frames of State Contract No. FFUF-2024-0021 using the facilities of Center “Physics and Technology of Micro and Nanostructures” at IPM RAS.

-
- [1] A. N. Mahmoud, F. Vanderveken, F. Ciubotaru, C. Adelman, S. Hamdioui, and S. Cotozana, A spin wave-based approximate 4: 2 compressor: Seeking the most energy-efficient digital computing paradigm, *IEEE Nanotechnology Magazine* **16**, 47 (2021).
 - [2] U. Garlando, Q. Wang, O. V. Dobrovolskiy, A. V. Chumak, and F. Riente, Numerical model for 32-bit magnonic ripple carry adder, *IEEE Transactions on Emerging Topics in Computing* **11**, 679 (2023).
 - [3] A. Mahmoud, F. Ciubotaru, F. Vanderveken, A. V. Chumak, S. Hamdioui, C. Adelman, and S. Cotozana, Introduction to spin wave computing, *Journal of Applied Physics* **128**, 10.1063/5.0019328 (2020).
 - [4] Q. Wang, M. Kewenig, M. Schneider, R. Verba, F. Kohl, B. Heinz, M. Geilen, M. Mohseni, B. Lagel, F. Ciubotaru, *et al.*, A magnonic directional coupler for integrated magnonic half-adders, *Nature Electronics* **3**, 765 (2020).
 - [5] K. Szulc, P. Graczyk, M. Mruczkiewicz, G. Gubbiotti, and M. Krawczyk, Spin-wave diode and circulator based on unidirectional coupling, *Physical Review Applied* **14**, 034063 (2020).
 - [6] G. Talmelli, T. Devolder, N. Trager, J. Forster, S. Wintz, M. Weigand, H. Stoll, M. Heyns, G. Schutz, I. P. Radu, *et al.*, Reconfigurable submicrometer spin-wave majority gate with electrical transducers, *Science Advances* **6**, eabb4042 (2020).
 - [7] . Papp, W. Porod, and G. Csaba, Nanoscale neural network using non-linear spin-wave interference, *Nature communications* **12**, 6422 (2021).
 - [8] S. Watt, M. Kostylev, and A. B. Ustinov, Enhancing computational performance of a spin-wave reservoir computer with input synchronization, *Journal of Applied Physics* **129**, 10.1063/5.0033292 (2021).
 - [9] M. Balynsky, H. Chiang, D. Gutierrez, A. Kozhevnikov, Y. Filimonov, and A. Khitun, Quantum computing without quantum computers: Database search and data processing using classical wave superposition, *Journal of Applied Physics* **130**, 10.1063/5.0068316 (2021).
 - [10] A. Mahmoud, N. Cucu-Laureciu, F. Vanderveken, F. Ciubotaru, C. Adelman, S. Cotozana, and S. Hamdioui, Would magnonic circuits outperform CMOS counterparts?, in *Proceedings of the Great Lakes Symposium on VLSI 2022* (2022) pp. 309–313.
 - [11] A. Barman, G. Gubbiotti, S. Ladak, A. O. Adeyeye, M. Krawczyk, J. Grafe, C. Adelman, S. Cotozana, A. Naeemi, V. I. Vasyuchka, *et al.*, The 2021 magnonics roadmap, *Journal of Physics: Condensed Matter* **33**, 413001 (2021).
 - [12] P. Delsing, A. N. Cleland, M. J. Schuetz, J. Knorzer, G. Giedke, J. I. Cirac, K. Srinivasan, M. Wu, K. C. Balram, C. Bauerle, *et al.*, The 2019 surface acoustic waves roadmap, *Journal of Physics D: Applied Physics* **52**, 353001 (2019).
 - [13] V. Vlasov, A. Golov, L. Kotov, V. Shcheglov, and V. Temnov, The modern problems of ultrafast magnetoacoustics (review), *Acoustical Physics* **68**, 18 (2022).

- [14] W.-G. Yang and H. Schmidt, Acoustic control of magnetism toward energy-efficient applications, *Applied Physics Reviews* **8**, 021304 (2021).
- [15] Y. Li, C. Zhao, W. Zhang, A. Hoffmann, and V. Novosad, Advances in coherent coupling between magnons and acoustic phonons, *APL Materials* **9**, 060902 (2021).
- [16] A. A. Bukharaev, A. K. Zvezdin, A. P. Pyatakov, and Y. K. Fetisov, Straintronics: a new trend in micro-and nanoelectronics and materials science, *Physics-Uspekhi* **61**, 1175 (2018).
- [17] K. Yamamoto, M. Xu, J. Puebla, Y. Otani, and S. Maekawa, Interaction between surface acoustic waves and spin waves in a ferromagnetic thin film, *Journal of Magnetism and Magnetic Materials* **545**, 168672 (2022).
- [18] N. K. Babu, A. Trzaskowska, P. Graczyk, G. Centala, S. Mieszczyk, H. Glowinski, M. Zdunek, S. Mielcarek, and J. W. Klos, The interaction between surface acoustic waves and spin waves: The role of anisotropy and spatial profiles of the modes, *Nano letters* **21**, 946 (2020).
- [19] Y. Hwang, J. Puebla, K. Kondou, C. Gonzalez-Ballester, H. Ishiki, C. S. Muñoz, L. Liao, F. Chen, W. Luo, S. Maekawa, and Y. Otani, Strongly coupled spin waves and surface acoustic waves at room temperature, *Phys. Rev. Lett.* **132**, 056704 (2024).
- [20] D. D. Yaremkevich, A. V. Scherbakov, L. De Clerk, S. M. Kukhtaruk, A. Nadzeyka, R. Campion, A. W. Rushforth, S. Savel'ev, A. G. Balanov, and M. Bayer, On-chip phonon-magnon reservoir for neuromorphic computing, *Nature Communications* **14**, 8296 (2023).
- [21] M. Bombeck, A. S. Salasyuk, B. A. Glavin, A. V. Scherbakov, C. Brüggemann, D. R. Yakovlev, V. F. Sapega, X. Liu, J. K. Furdyna, A. V. Akimov, and M. Bayer, Excitation of spin waves in ferromagnetic (Ga,Mn)As layers by picosecond strain pulses, *Phys. Rev. B* **85**, 195324 (2012).
- [22] Y. Hashimoto, D. Bossini, T. H. Johansen, E. Saitoh, A. Kirilyuk, and T. Rasing, Frequency and wavenumber selective excitation of spin waves through coherent energy transfer from elastic waves, *Phys. Rev. B* **97**, 140404 (2018).
- [23] B. Casals, N. Statuto, M. Foerster, A. Hernández-Mínguez, R. Cicheler, P. Manshausen, A. Mandziak, L. Aballe, J. M. Hernández, and F. Macià, Generation and imaging of magnetoacoustic waves over millimeter distances, *Phys. Rev. Lett.* **124**, 137202 (2020).
- [24] M. Küß, M. Heigl, L. Flacke, A. Hörner, M. Weiler, M. Albrecht, and A. Wixforth, Nonreciprocal Dzyaloshinskii-Moriya magnetoacoustic waves, *Phys. Rev. Lett.* **125**, 217203 (2020).
- [25] T. Hioki, Y. Hashimoto, and E. Saitoh, Coherent oscillation between phonons and magnons, *Communications Physics* **5**, 115 (2022).
- [26] I. A. Filatov, P. I. Gerevenkov, A. V. Azovtsev, V. A. Kovaleva, N. E. Khokhlov, and A. M. Kalashnikova, Magnon-Cherenkov effect from a picosecond strain pulse, PREPRINT (Version 1) available at Research Square 10.21203/rs.3.rs-5971617/v1 (2025).
- [27] See supplemental material at [url will be inserted by publisher] for details of simulation, static magnetisation distribution, and symmetrical propagation of the waves at round spot excitation.
- [28] N. E. Khokhlov, P. I. Gerevenkov, L. A. Shelukhin, A. V. Azovtsev, N. A. Pertsev, M. Wang, A. W. Rushforth, A. V. Scherbakov, and A. M. Kalashnikova, Optical excitation of propagating magnetostatic waves in an epitaxial galferol film by ultrafast magnetic anisotropy change, *Physical Review Applied* **12**, 044044 (2019).
- [29] M. Jäckl, V. Belotelov, I. Akimov, I. Savochkin, D. Yakovlev, A. Zvezdin, and M. Bayer, Magnon accumulation by clocked laser excitation as source of long-range spin waves in transparent magnetic films, *Physical Review X* **7**, 021009 (2017).
- [30] A. Vansteenkiste, J. Leliaert, M. Dvornik, M. Helsen, F. Garcia-Sanchez, and B. Van Waeyenbergh, The design and verification of mumax3, *AIP advances* **4**, 107133 (2014).
- [31] I. A. Filatov, P. Gerevenkov, M. Wang, A. Rushforth, A. Kalashnikova, and N. Khokhlov, Spectrum evolution and chirping of laser-induced spin wave packets in thin iron films, *Applied Physics Letters* **120**, 10.1063/5.0077195 (2022).
- [32] I. Viktorov, *Rayleigh and Lamb Waves: Physical Theory and Applications*, Ultrasonic Technology (Springer US, 2013).
- [33] A. Tarasenko, R. Čtvrtlík, and R. Kudělka, Theoretical and experimental revision of surface acoustic waves on the (100) plane of silicon, *Scientific Reports* **11**, 10.1038/s41598-021-82211-6 (2021).
- [34] T. Saito, O. Matsuda, M. Tomoda, and O. B. Wright, Imaging gigahertz surface acoustic waves through the photoelastic effect, *J. Opt. Soc. Am. B* **27**, 2632 (2010).
- [35] Y. Sugawara, O. B. Wright, O. Matsuda, M. Takigahira, Y. Tanaka, S. Tamura, and V. E. Gusev, Watching ripples on crystals, *Phys. Rev. Lett.* **88**, 185504 (2002).
- [36] G. Farnell and E. Adler, 2 - elastic wave propagation in thin layers, in *Physical Acoustics Principles and Methods*, Physical Acoustics, Vol. 9, edited by W. P. Mason and R. N. Thurston (Academic Press, 1972) pp. 35–127.
- [37] C. Berk, M. Jaris, W. Yang, S. Dhuey, S. Cabrini, and H. Schmidt, Strongly coupled magnon-phonon dynamics in a single nanomagnet, *Nature communications* **10**, 2652 (2019).
- [38] M. Yan, A. Kakay, C. Andreas, and R. Hertel, Spin-Cherenkov effect and magnonic mach cones, *Physical Review B* **88**, 220412 (2013).
- [39] J. Xia, X. Zhang, M. Yan, W. Zhao, and Y. Zhou, Spin-Cherenkov effect in a magnetic nanostrip with interfacial Dzyaloshinskii-Moriya interaction, *Scientific reports* **6**, 25189 (2016).
- [40] O. Dobrovolskiy, Q. Wang, D. Y. Vodolazov, B. Budinska, S. Knauer, R. Sachser, M. Huth, and A. Buzdin, Cherenkov radiation of spin waves by ultra-fast moving magnetic flux quanta, *arXiv preprint arXiv:2103.10156* 10.48550/arXiv.2103.10156 (2021).
- [41] A. V. Sadovnikov, C. S. Davies, S. V. Grishin, V. Kruglyak, D. Romanenko, Y. P. Sharaevskii, and S. Nikitov, Magnonic beam splitter: The building block of parallel magnonic circuitry, *Applied Physics Letters* **106**, 10.1063/1.4921206 (2015).
- [42] A. Martyshkin, S. Sheshukova, F. Ogrin, E. Lock, D. Romanenko, S. Nikitov, and A. Sadovnikov, Nonreciprocal spin-wave beam transport in a metallized T-shaped magnonic junction, *Physical Review Applied* **22**, 014037 (2024).
- [43] C. Davies, A. Francis, A. Sadovnikov, S. Chertopalov, M. Bryan, S. Grishin, D. Allwood, Y. P. Sharaevskii, S. Nikitov, and V. Kruglyak, Towards graded-index magnonics: Steering spin waves in magnonic networks,

- Physical Review B **92**, 020408 (2015).
- [44] P. Carrara, M. Brioschi, R. Silvani, A. Adeyeye, G. Panaccione, G. Gubbiotti, G. Rossi, and R. Cucini, Coherent and dissipative coupling in a magnetomechanical system, Physical Review Letters **132**, 216701 (2024).
- [45] A. Trzaskowska, P. Graczyk, N. Babu, M. Zdunek, H. Głowiński, J. Kłos, and S. Mielcarek, The studies on phonons and magnons in [cofeb/au] n multilayers of different number of repetitions, Journal of Magnetism and Magnetic Materials **549**, 169049 (2022).